# Equilibrium Polarization of Ultrathin PbTiO_{3} with Surface Compensation Controlled by Oxygen Partial Pressure

M. J. Highland, T. T. Fister, D. D. Fong, P. H. Fuoss, Carol Thompson, J. A. Eastman, S. K. Streiffer, and G. B. Stephenson

# Equilibrium Polarization of Ultrathin PbTiO$_3$ with Surface Compensation Controlled by Oxygen Partial Pressure

M.J. Highland,[1, *] T.T. Fister,[2] D.D. Fong,[1] P.H. Fuoss,[1] Carol Thompson,[3] J.A. Eastman,[1] S.K. Streiffer,[4] and G.B. Stephenson[1]

[1]*Materials Science Division, Argonne National Laboratory, Argonne, Illinois 60439, USA*
[2]*Chemical Sciences and Engineering Division, Argonne National Laboratory, Argonne, Illinois 60439, USA*
[3]*Department of Physics, Northern Illinois University, DeKalb, Illinois 60115, USA*
[4]*Physical Sciences and Engineering Directorate, Argonne National Laboratory, Argonne, Illinois 60439, USA*

We present a synchrotron x-ray study of the *equilibrium* polarization structure of ultrathin PbTiO$_3$ films on SrRuO$_3$ electrodes epitaxially grown on SrTiO$_3$ (001) substrates, as a function of temperature and the external oxygen partial pressure ($p$O$_2$) controlling their surface charge compensation. We find that the ferroelectric Curie temperature ($T_C$) varies with $p$O$_2$, and has a minimum at the intermediate $p$O$_2$ where the polarization below $T_C$ changes sign. The experiments are in qualitative agreement with a model based on Landau theory that takes into account the interaction of the phase transition with the electrochemical equilibria for charged surface species. The paraelectric phase is stabilized at intermediate $p$O$_2$ when the concentrations of surface species are insufficient to compensate either polar orientation.

The presence of a phase transition between nonpolar and polar states in ferroelectric materials is responsible for their fascinating and useful properties such as divergent dielectric susceptibility, outstanding piezoelectric and pyroelectric coefficients, and ability to be switched between different stable polarization orientations through the momentary application of a field [1, 2]. Recent studies have found that the extent of the compensation of the polarization by free charge at interfaces strongly affects the phase transition and thus the properties of ultrathin ferroelectric films and nanostructures [3–6]. Incomplete charge compensation due to finite electronic screening lengths in electrodes results in a residual depolarizing field and a reduction in the Curie temperature $T_C$ [7–9]. Insufficiently compensated interfaces can result in the appearance of equilibrium 180° stripe domain and vortex polarization structures [5, 6, 10–13]. Competitions between energy terms that scale with surface area and those that scale with volume result in large changes to the behavior as the system size decreases.

Charge compensation of ferroelectric surfaces without electrodes can involve extra or missing ions arising from interaction with the environment, rather than electrons [14–21]. Sufficient ionic compensation can occur so that ultrathin films remain polar [15, 16, 22], and their polarization orientation can be controlled by changing the chemistry of the environment [17, 20]. When the polarization orientation of PbTiO$_3$ films is inverted by changing the external oxygen partial pressure controlling ionic compensation, recent experiments [21] have found that, depending upon film thickness and temperature, the transition can occur either through the nucleation and growth of inverted domains or by a continuous mechanism, in which the polarization uniformly decreases to zero and inverts without the formation of domains. This crossover could be explained as an effect of either kinetics (e.g. limited nucleation rate) or thermodynamics (e.g. limited phase stability) in ultrathin films [21]. While first-principles theory [15, 17–19] has confirmed that ionic compensation of surfaces is expected to be sufficient to stabilize polar phases in ultra-

thin ferroelectric films, the simple extrapolations used to apply these results to nonzero temperatures have not taken into account the ferroelectric phase transition. To date most experiments on ultrathin ferroelectrics have been performed either in air [15, 22–26] or in vacuum conditions [3, 26–28], often without accounting for the possible large difference in equilibrium polarization stability. These considerations motivate the present work, the first determination of the *equilibrium* polarization phase diagrams of ultrathin ferroelectric films as a function of temperature and the external chemical potential controlling their ionic surface compensation.

Here we study epitaxial heterostructures consisting of ferroelectric PbTiO$_3$ (001) layers on conducting SrRuO$_3$ layers, both fully lattice-matched to SrTiO$_3$ single crystal substrates. This epitaxy constrains the PbTiO$_3$ polarization orientation in the film to be normal to the surface at the temperatures investigated [21, 29]. The top surface of the PbTiO$_3$ is compensated by extra or missing oxygen ions produced by interaction with the environment – a controlled oxygen partial pressure ($p$O$_2$) in a flowing N$_2$ ambient at 13 mbar total pressure – while the bottom is compensated by electronic charge in the SrRuO$_3$. The films are grown following procedures described elsewhere [15, 17, 21]. Grazing incidence x-ray scattering is used to characterize the atomic positions in the heterostructure. X-ray measurements are performed *in situ* in the chamber used for PbTiO$_3$ film growth, at beamline 12ID-D of the Advanced Photon Source [17, 21]. Values for the PbTiO$_3$ lattice parameter $c$ and positive domain fraction $x_{pos}$ are obtained by fitting the measured intensities along the $30L$ crystal truncation rod (CTR) using the calculated scattering from an atomic-scale model of the PbTiO$_3$/SrRuO$_3$/SrTiO$_3$ heterostructure as described previously [17, 21]. The local polarization magnitude $|P|$ is obtained from $c$ using the well established relationship between strain and polarization in PbTiO$_3$ [29, 30]. For each value of $p$O$_2$, data is obtained at successively lower temperatures by cooling from the nonpolar phase. In performing these experiments at constant $p$O$_2$, we find no significant depen-
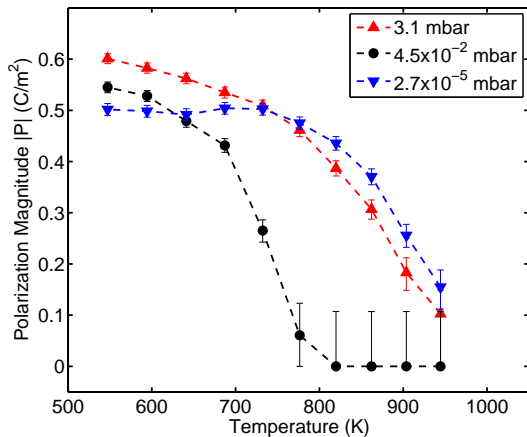
FIG. 1: (Color online) Polarization magnitude vs. temperature for a 5-nm-thick PbTiO$_3$ film on SrRuO$_3$ coherently strained to SrTiO$_3$ at three $p$O$_2$ values. The temperature below which the film polarizes ($T_C$) is significantly lower at the intermediate $p$O$_2$.

dence of the results upon whether a temperature is approached from above or below, in contrast to the large hysteresis observed when the film polarization orientation is switched by changing $p$O$_2$ at constant $T$ [17, 21]. Thus a better determination of the equilibrium states is obtained by changing $T$ at constant $p$O$_2$.

The measurements show that the temperature dependence of the PbTiO$_3$ polarization is a strong function of the external $p$O$_2$. Figure 1 shows $|P|$ versus $T$ for a 5 nm PbTiO$_3$ film at three $p$O$_2$ values. The Curie temperature $T_C$ below which the film polarizes is strongly suppressed at the intermediate $p$O$_2$ value. Values of $c$, $x_{pos}$, and $|P|$ as a function of $T$ and $p$O$_2$ for 10-, 5-, and 3.5-nm-thick PbTiO$_3$ films are given in supplemental material [31]. These have been assembled to create the equilibrium phase diagrams shown in Fig. 2. Here the color scale represents the net polarization $\langle P \rangle \equiv |P|(2x_{pos} - 1)$, while the symbols show the phase observed at each point measured [31]. At lower $T$, the polarization has opposite sign for high and low $p$O$_2$ ($x_{pos} = 1$ and 0, respectively). The observed $T_C$ (solid line) is minimum at the $p$O$_2$ value where the polarization orientation below $T_C$ changes sign. The degree to which $T_C$ is suppressed at these intermediate $p$O$_2$ values becomes greater as film thickness decreases. The square symbols show points where the CTR fitting indicates a mixed domain structure with $0.13 < x_{pos} < 0.87$. At these points we typically observe diffuse scattering satellite peaks in the in-plane directions around the Bragg peak, indicating formation of equilibrium 180° stripe domains with periods in the range 12-25 nm [10, 11].

The data presented in Figs. 1 and 2 are for a TiO$_2$ surface termination of the PbTiO$_3$, which we created at high temperature after growth by reducing the PbO vapor pressure in the chamber below the value that stabilizes the PbO surface termination [32]. We obtained a less extensive dataset for the
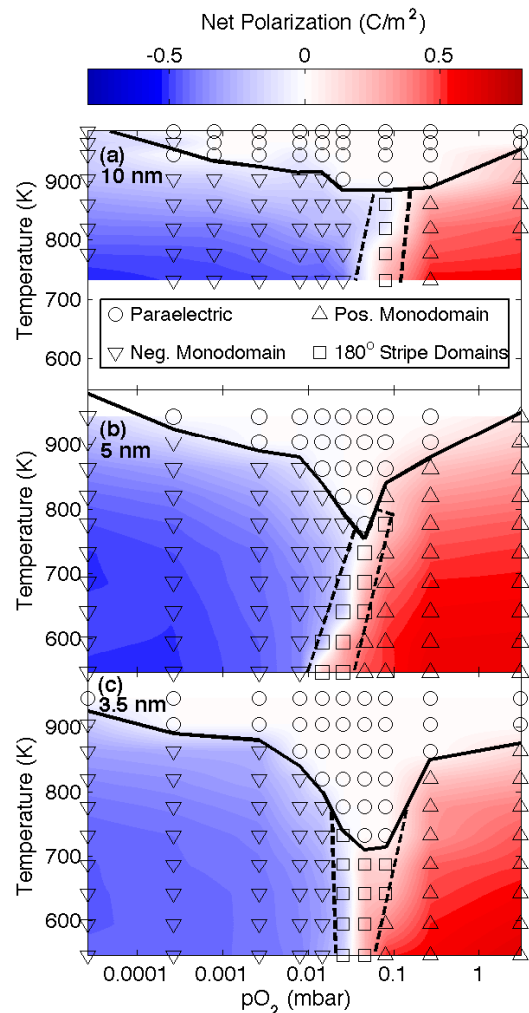


FIG. 2: (Color online) Temperature vs. $p$O$_2$ phase diagrams for three thicknesses of PbTiO$_3$ on SrRuO$_3$ coherently strained to SrTiO$_3$ (001). Color scale indicates net polarization. Symbols show points measured and phase observed. Solid lines indicate $T_C$, and dashed lines are boundaries of 180° stripe domain regions.

PbO surface termination, which we found to be more difficult to maintain consistently under all conditions for the length of time required for measurements (e.g. 1 hour per condition). The phase diagrams for both terminations are quite similar, with a minimum $T_C$ at the $p$O$_2$ of the transition between positive and negative polar phases. For the 5 nm film, the PbO-terminated surface has a minimum $T_C$ that is approximately 8 K lower and occurs a factor of 1.4 lower in $p$O$_2$ than the TiO$_2$-terminated surface.

While previous work [17, 21] showed that the polarization orientation in ultrathin films could be inverted by changing between high and low $p$O$_2$, the equilibrium results in Figs. 1 and 2 show that applied oxygen potential is not equivalent to applied electric potential. Because PbTiO$_3$ coherently strained to SrTiO$_3$ has a second-order transition at zero field [29], if it were cooled under a nonzero applied electric field the polarization would be expected to increase continuously without
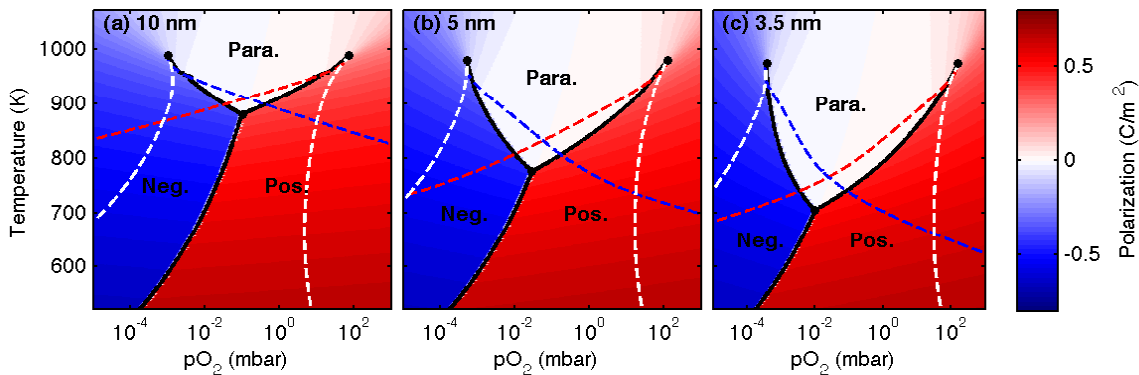
FIG. 3: (Color online) Predicted polarization phase diagrams as a function of temperature and $pO_2$ for three thicknesses of PbTiO$_3$ on SrRuO$_3$ coherently strained to SrTiO$_3$ (001), from theory for ferroelectric films with ionic compensation [30]. Solid curves show equilibrium phase boundaries, and dashed red, blue, and white curves show metastability limits for the positive, negative, and paraelectric phases, respectively.

crossing a phase boundary between nonpolar and polar states [30]. Here we see a clear phase transition when cooling at each $pO_2$, with a $T_C$ that varies with $pO_2$.

The experimental results can be qualitatively understood by considering the equilibrium concentrations of extra or missing surface ions and their interaction with the film polarization. Calculations using a model [30] based on Landau-Ginzburg-Devonshire theory for the ferroelectric phase transition supplemented by electrochemical equilibria for charged surface species are shown in Fig. 3. The Gibbs free energy per unit area is written as [30]

$$
\begin{aligned}
\mathcal{G} = & \; t \left[ f(P) + \frac{(\sigma + P)^2}{2\epsilon_0} \right] + \frac{\lambda^\dagger \sigma^2}{\epsilon_0} \\
& + \sum_{i=\ominus,\oplus} \frac{kT}{A} \left[ \frac{\theta_i \Delta G_i^{\circ\circ}}{kT} - \frac{\theta_i \ln pO_2}{n_i} \right. \\
& \left. + \; \theta_i \ln \theta_i + (1 - \theta_i) \ln(1 - \theta_i) \right],
\end{aligned}
\tag{1}
$$

where $t$ is the ferroelectric film thickness, $P$ is the polarization (assumed normal to the film surface), $f(P)$ is the standard Landau expansion of the free energy, $\sigma$ is the compensating surface charge density, $\lambda^\dagger$ is the effective compensation screening length, $A$ is the surface area per ion site, $\theta_i$ is the surface concentration of negative or positive species $i = \ominus$ or $\oplus$, and $\Delta G_i^{\circ\circ}$ is their standard free energy of formation from $n_i^{-1}$ O$_2$ molecules. The surface charge is related to the ion concentrations by $\sigma = \sum_i z_i e \theta_i / A$, where $z_i e$ is the ionic charge. Minimization of this free energy with respect to $P$ and the $\theta_i$ yields the equilibrium polarization phase diagrams shown in Fig. 3, using the parameters in Table I. The values of $n_i$ and $z_i$ are consistent with doubly-charged oxygen anions and vacancies as the negative and positive surface species, respectively, which have been found to stabilize monodomain polarization in *ab initio* calculations [15, 17]. Note that the effective screening length $\lambda^\dagger$ can be negative in this model [30] because it includes a term from the polarization dependence of the ion formation energies.

TABLE I: Values of coefficients used in Fig. 3.

| $\Delta G_\oplus^{\circ\circ}$ | 0.87 | (eV) | $\Delta G_\ominus^{\circ\circ}$ | 0.17 | (eV) |
|---|---|---|---|---|---|
| $n_\oplus$ | $-2$ | | $n_\ominus$ | 2 | |
| $z_\oplus$ | 2 | | $z_\ominus$ | $-2$ | |
| $A$ | $3.2 \times 10^{-19}$ | (m$^2$) | $\lambda^\dagger$ | $-1 \times 10^{-12}$ | (m) |

The model qualitatively reproduces the observed minimum in $T_C$ at an intermediate $pO_2$ value (where a triple point occurs between positive polar, negative polar, and paraelectric phases), as well as the increasing depth of this minimum as film thickness becomes smaller. This stabilization of the paraelectric phase occurs because at these $pO_2$ values, the surface ionic charge density is too low to compensate either polar state. The model also predicts a tilting of the positive/negative phase boundary below $T_C$ towards lower $pO_2$ at lower $T$, for which there is some evidence in the experimental data. The model assumes that the film polarization is uniform, and so does not capture the equilibrium 180° stripe domains that are observed along this boundary. While the terms in the sum in Eq. (1) used in the model produce transitions between the paraelectric and polar phases that are first order [30], the lack of a discontinuity in the measured $P(T)$ curves indicates that they may actually be second order. Alternatively, this may be an averaging of $T_C$ due to inevitable nonuniformity of the film thickness on the single-unit-cell (0.4 nm) scale.

These results provide an explanation for the recent observation [21] of polarization switching without domain formation at the intrinsic coercive field in sufficiently thin PbTiO$_3$ films. Figure 4 shows the observed film thickness and temperature diagram [21] giving the regions for which polarization switching by changing $pO_2$ at constant temperature occurs by nucleation of oppositely polarized domains, or alternatively by a continuous mechanism in which the local polarization magnitude passes through zero. Superimposed upon this diagram are three points corresponding to the minimum $T_C$ from Fig. 2 for the three film thicknesses studied here. They cor-
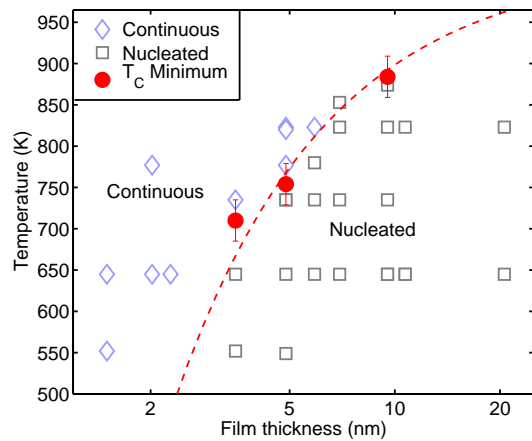
FIG. 4: (Color online) Correspondence between regions of continuous and nucleated switching mechanisms found previously (open symbols) [21], and the minimum $T_C$ observed in this work (solid circles). Dashed curve is a fit to $T_C^{min} = T_C^{\circ}(1 - t^*/t)$, where $T_C^{\circ} = 1023$ K is the zero-field $T_C$ of PbTiO$_3$ coherently strained to SrTiO$_3$ [30], and $t^* = 1.2$ nm is the best fit value.

respond well with the boundary between the continuous and nucleated mechanisms of switching. This agreement implies that the change in switching mechanism occurs because of equilibrium behavior rather than simply kinetic effects – the continuous mechanism occurs when, at the $pO_2$ where the parent polar phase loses stability, the stable phase is the nonpolar phase rather than the oppositely polarized or stripe phase. The instability curves shown on the calculated phase diagrams in Fig. 3 indicate that such regions can exist. If the transition is second order at $T_C$, then the instabilities would coincide with the phase boundaries. Furthermore, the internal field is predicted to reach the intrinsic coercive field at these instabilities. On the other hand, the regions of equilibrium 180° stripe domains on the phase diagrams of Fig. 2 indicate that the nucleated switching mechanism observed at these lower temperatures may occur through the initial formation of stripe domains.

These studies show that the chemical environment at the surface of an ultrathin ferroelectric film has strong effects on its phase transition. The nonpolar phase is stabilized and $T_C$ is suppressed at intermediate chemical potentials where the concentrations of surface species are insufficient to compensate either orientation of the polar phase. Such ionic compensation offers a new tool for tuning ferroelectric properties and a new avenue for devices, and must be considered when comparing studies carried out in different environments, e.g. ambient air or vacuum. While these results are for ionic compensation of surfaces, similar effects should occur at buried interfaces, such as that between a ferroelectric and an ionic conductor. Further development of the theory for ionic compensation and its validation through experiment will lay the ground work for fully understanding how a ferroelectric thin film interacts with its environment, and for fully realizing the potential of ferroelectric materials.

* Electronic mail: mhighland@anl.gov

[1] R. Ramesh and D. G. Schlom, *MRS Bulletin* **33**, 1006 (2008).

[2] M. Dawber, K. M. Rabe, and J. F. Scott, *Rev. Mod. Phys.* **77**, 1083 (2005).

[3] M. F. Chisholm, W. Luo, M. P. Oxley, S. T. Pantelides, and H. N. Lee, *Phys. Rev. Lett.* **105**, 197602 (2010).

[4] A. M. Kolpak *et al.*, *Phys. Rev. Lett.* **105**, 217601 (2010).

[5] P. Zubko, N. Stucki, C. Lichtensteiger, and J.-M. Triscone, *Phys. Rev. Lett.* **104**, 187601 (2010).

[6] M. G. Stachiotti and M. Sepliarsky, *Phys. Rev. Lett.* **106**, 137601 (2011).

[7] I. P. Batra, P. Wurfel, and B. D. Silverman, *Phys. Rev. Lett.* **30**, 384 (1973).

[8] N. Sai, A. M. Kolpak, and A. M. Rappe, *Phys. Rev. B* **72**, 020101(R) (2005).

[9] M. Stengel, D. Vanderbilt, and N. A. Spaldin, *Nature Mater.* **8**, 392 (2009).

[10] S. K. Streiffer *et al.*, *Phys. Rev. Lett.* **89**, 067601 (2002).

[11] D. D. Fong *et al.*, *Science* **304**, 1650 (2004).

[12] B.-K. Lai, I. Ponomareva, I. Kornev, L. Bellaiche, and G. Salamo, *Appl. Phys. Lett.* **91**, 152909 (2007).

[13] C. Thompson *et al.*, *Appl. Phys. Lett.* **93**, 182901 (2008).

[14] S. V. Kalinin and D. A. Bonnell, *Nano Lett.* **4**, 555 (2004).

[15] D. D. Fong *et al.*, *Phys. Rev. Lett.* **96**, 127601 (2006).

[16] R. Takahashi *et al.*, *Appl. Phys. Lett.* **92**, 112901 (2008).

[17] R. V. Wang *et al.*, *Phys. Rev. Lett.* **102**, 047601 (2009).

[18] J. Shin *et al.*, *Nano Lett.* **9**, 3720 (2009).

[19] N. C. Bristowe, M. Stengel, P. B. Littlewood, J. M. Pruneda, and E. Artacho, http://arxiv.org/abs/1108.2208v1.

[20] Y. Kim, I. Vrejoiu, D. Hesse, and M. Alexe, *Appl. Phys. Lett.* **96**, 202902 (2010).

[21] M. J. Highland *et al.*, *Phys. Rev. Lett.* **105**, 167601 (2010).

[22] C. Lichtensteiger, J.-M. Triscone, J. Junquera, and P. Ghosez, *Phys. Rev. Lett.* **94**, 047603 (2005).

[23] C. Thompson, C. M. Foster, J. A. Eastman, and G. B. Stephenson, *Appl. Phys. Lett.* **71**, 3516 (1997).

[24] D. D. Fong *et al.*, *Phys. Rev. B* **71**, 144112 (2005).

[25] S. V. Kalinin *et al.*, *Phys. Rev. Lett.* **100**, 155703 (2008).

[26] P. Maksymovych *et al.*, *Phys. Rev. Lett.* **102**, 017601 (2009).

[27] M. J. Bedzyk *et al.*, *Phys. Rev. B* **61**, R7873 (2000).

[28] L. Despont *et al.*, *Phys. Rev. B* **73**, 094110 (2006).

[29] N. A. Pertsev, A. G. Zembilgotov, and A. K. Tagantsev, *Phys. Rev. Lett.* **80**, 1988 (1998).

[30] G. B. Stephenson and M. J. Highland, *Phys. Rev. B* **84**, 064107 (2011).

[31] See supplementary material at http://link.aps.org/ supplemental/11.xxxx/PhysRevLett.107.yyyyyy for tables of $c$ and $x_{pos}$ obtained from fits and derived values of $|P|$ and $\langle P \rangle$.

[32] A. Munkholm *et al.*, *Phys. Rev. Lett.* **88**, 016101 (2001).